Mechanisms of Photochemistry and Reactive Oxygen Production by Fullerene Suspensions in Water

ERNEST M. HOTZE,[†] JEROME LABILLE,[‡] PEDRO ALVAREZ,[§] AND MARK R. WIESNER*,[†]

Department of Civil and Environmental Engineering, Duke University, Durham, North Carolina 27708-0287, CEREGE, University Aix-Marseille, Aix-en-Provence, France, and Department of Civil and Environmental Engineering, Rice University, Houston, Texas 77251-1892

Received August 29, 2007. Revised manuscript received January 13, 2008. Accepted March 12, 2008.

Buckminsterfullerene (C_{60}) is a known photosensitizer that produces reactive oxygen species (ROS) in the presence of light; however, its properties in aqueous environments are still not well understood or modeled. In this study, production of both singlet oxygen and superoxide by UV photosensitization of colloidal aggregates of C_{60} in water was measured by two distinct methods: electron paramagnetic resonance (EPR) with a spin trapping compound, and spectrophotometric detection of the reduced form of the tetrazolium compound XTT. Both singlet oxygen and superoxide were generated by fullerol suspensions while neither was detected in the aqu/nC_{60} suspensions. A mechanistic framework for photosensitization that takes into account differences in C_{60} aggregate structure in water is proposed to explain these results. While theory developed for single molecules suggests that alterations to the C_{60} cage should reduce the quantum yield for the triplet state and associated ROS production, the failure to detect ROS production by aqu/nC_{60} is explained in part by a more dense aggregate structure compared with the hydroxylated C_{60}.

1. Introduction

Commercial products containing fullerenes are already on the market. These include tennis racquets (*1*), epidermal growth factor (*2*), and facial antioxidant cream (*3*) to name a few. The availability and use of these products and a substantial increase in production forecasted for fullerenes suggests that these materials may make their way into wastewater treatment influents and aquatic environments. The richness of organic chemistry allows for an uncountable number of fullerene variations through functionalization. Also, the behavior of these materials may be altered by the commercial and natural matrices in which they are immersed. However, an evaluation of the surface and photochemistry of some relatively simple aqueous suspensions of fullerenes is an essential starting point for assessing the environmental impacts of fullerenes and basis for benchmarking more complex systems.

* Corresponding author phone: 919-660-5292; fax: 919-660-5219; e-mail: wiesner@duke.edu.
[†] Duke University.
[‡] University Aix-Marseille.
[§] Rice University.

The properties of C_{60} and other fullerenes have been described in numerous studies with respect to fullerene toxicity (*4–8*), antioxidant capacity (*9–11*), and characterization (*12–15*). The ability of C_{60} to produce reactive oxygen species, or ROS, (e.g., (*16*)) has received considerable attention, in part based on the implications for toxicity to cells (*5*) in both medical and environmental contexts as well as the potential applications implied for industrial or water treatment technologies (*17, 18*). However, unlike the conditions leading to ROS production via photosensitization by individual C_{60} molecules in organic solvent, (*19, 20*), the conditions that lead to ROS production by C_{60} in water and the reactive species formed are less well understood. We have previously reported on the ability of hydroxylated C_{60} (fullerol) to produce ROS in water (*17, 18*), but have not considered the ROS speciation and underlying mechanisms.

Photosensitized molecules like fullerene are capable of transferring light energy to chemical oxidation potential in the form of ROS. When the photosensitized molecule transfers energy directly to an oxygen molecule, ROS formation may occur via a type II pathway primarily resulting in singlet oxygen ($^1O_2$). Type I ROS formation occurs when photosensitization increases interactions between a photosensitizer molecule and an electron donor, ultimately leading to the transfer of an electron to an oxygen and the production of radicals such as superoxide ($O_2^{-\bullet}$). The efficiency of light energy transferred relative to the amount of ROS formed can be expressed as a quantum yield (*21*). Pristine fullerene suspended in a nonpolar solvent has a quantum yield near unity (*19*) indicating little to no loss of energy between initial photosensitization and formation of its triplet excited state ($^3C_{60}$). However the introduction of fullerenes into a polar solvent, such as water, results in a very different chemical environment and physical configuration of C_{60} compared with the organic solutions of C_{60} that have been the subject of previous studies of ROS formation. In particular, stable suspensions of fullerenes in water tend to be present as colloidal aggregates. Indeed, the study of ROS generation by fullerenes in water is complicated by the low solubility of many of these materials in water. Nonetheless, stable suspensions of these materials may be produced either intentionally or naturally through encapsulation (*22–25*), functionalization (*26–28*), or aggregation (*29–32*).

The degree to which fullerenes are functionalized appears to affect the tendency of these molecules to form aggregates. Monofunctionalized (*33*) molecules tend to aggregate despite functionalization (*34*), bis-functionalized fullerenes aggregate somewhat less due to steric hindrance, and poly functionalized fullerenes exhibit greater stability with respect to limited aggregation. Nonetheless, aggregation of poly functionalized C_{60} may readily occur and has been observed in some cases to increase with concentration (*15*), whereas in other cases, concentration does not seem to have an effect on aggregation (*35*). One of the more studied poly functionalized fullerenes is a hydroxylated form known as fullerol which can have a varying amount of hydroxyl groups on its surface depending on reaction conditions (*26*). Even with this surface modification, fullerol forms colloidal aggregates in suspensions that are stable to a maximum concentration of approximately 38.5 mM (*15*), depending on the number of hydroxyl groups added.

Stable colloidal suspensions of initially unfunctionalized C_{60} can be made by extended stirring (*25, 31*) or sonication in water (aqu/nC_{60}) (*36*) or through solvent exchange using organic solvents such as tetrahydrofuran (*12, 29*), or toluene (*37*). However, these latter colloidal suspensions of C_{60} may

10.1021/es702172w CCC: $40.75
Published on Web 04/29/2008

contain residual quantities of the organic solvent (*13*). Differences in the aggregation state of C_{60} as well as functionalization of the C_{60} contained within these aggregates may affect the ability of suspensions of these aggregates to produce ROS (*38*). One premise examined in this paper is that a higher proximity of two C_{60} cages within a dense aggregate may decrease ROS production by increasing the likelihood of processes such as triplet–triplet annihilation and self-quenching. In addition, dense aggregates will expose less of the fullerene to the solution, potentially reducing the active surface area for ROS production. In this study, we compare ROS production by two colloidal suspensions of C_{60} having very different aggregate structures as quantified by X-ray diffraction, aqu/nC_{60} and fullerol. We further differentiate conditions favoring type I and type II photosensitization reactions by these two suspensions.

2. Materials and Methods

2.1. Chemicals. Fullerol ($C_{60}(OH)_{22-24}$), and C_{60} (99.9% pure) were purchased from MER (Tucson, AZ). Superoxide dismutase (bovine ethrocytes) (SOD), 5,5-dimethyl-1-pyrroline-1-oxide (DMPO), 2,2,6,6-tetramethyl-4-piperidinol (4-oxo-TEMPO), Adenosine 5′-(trihydrogen diphosphate) (NADH), 2,2,6,6-tetramethyl-4-piperidone (TEMP), β-carotene, and XTT (2,3-bis(2-methoxy-4-nitro-5-sulfophenyl)-2H-tetrazolium-5-carboxanilide) were obtained from Sigma-Aldrich (St. Louis, MO). Deuterium Oxide (D_2O) was purchased from Cambridge Isotope Laboratories (Andover, MA). Ultrapure water had resistivity greater than 10 MΩ cm and dissolved organic carbon concentration <3 μg/L.

2.2. Irradiation. Irradiation was performed with both low and medium pressure UV lamps. Low pressure (LP) UV irradiation was done in the presence of two 15 W fluorescent ultraviolet bulbs (Philips TLD 15W/ 08). These bulbs have an output spectrum peak at 365 nm and a total irradiance of 24.1 W/m^2 (*17*). For singlet oxygen measurements irradiation by a low pressure (LP) UV light source was necessary for proximity to the EPR equipment.

Medium pressure (MP) irradiation (Calgon Carbon Corporation Pittsburgh, PA) was provided by a bench scale collimated beam (*39*). These experiments were carried out in a Petri dish with known sample depth and surface area allowing for a calculation of UV fluence (mJ/cm (*2*)). A UV radiometer and detector (International Light Inc., model 1700/SED 240/W) calibrated at 2 nm intervals in the range of 200−400 nm was used to measure UV irradiance at the top of the suspension. UV fluence (mJ/cm^2) was calculated as the average irradiance multiplied by the exposure time. The average UV irradiance in the completely mixed sample was determined from the incident irradiance, UV absorbance, and sample depth using an integrated form of the Beer–Lambert law. Utilizing a shutter, samples of various concentrations were exposed to UV light for 5 minute time intervals under the broadband MP UV source, the fluence was calculated as the total UV output in the 200−300 nm region. UV fluence was used as a normalizing factor in determining the capacity of each suspension to produce superoxide radicals. It should be noted that light under 300 nm in wavelength is more relevant to engineered systems rather than natural systems. Wavelengths larger than 300 nm are likely to be less effective in photosensitization. Our goal here, however, is to explore mechanisms of ROS formation by fullerenes rather than determine representative rates for either engineered or natural systems. Further study is needed to determine the rates of ROS that would occur in natural systems under typical solar illumination.

2.3. Instrumentation. EPR spectra were recorded at room temperature with a Varian E-6 spectrometer. The conditions for all measurements were: frequency, 9.27 GHz; power, 5 mW; modulation amplitude, 4 G; modulation frequency, 100 kHz. UV/vis spectrometry was preformed using a Hitachi U-2000 spectrophotometer. X-ray diffraction (XRD) was preformed using an X'Pert-Pro diffractometer from PANalytical instruments equipped with a Co anode source, and an RTMS scanning detector was used. Dynamic light scattering was preformed using a Zetasizer nano ZS (Malvern Instrument, Bedford, MA). This instrument employs a He−Ne laser (633 nm) and collects time variable scattering data at a fixed angle of 173°.

2.4. XRD Procedure. The structure of the C_{60} molecules in the fullerol and aqu/nC_{60} aggregates was characterized by X-ray scattering by samples prepared by depositing a few drops of aqu/nC_{60} or fullerol suspension on a silicon plate and allowing the water to evaporate. The 2 theta angle was continuously scanned from 10 to 90° with a 0.05° and 1 s. per step, and the divergence slit was automated so that a 10 mm sample length was constantly irradiated.

2.5. Singlet Oxygen Concentration Determination with EPR Spin Trapping. The spin-trapping reagent: 4-oxo-TEMP was used to trap singlet oxygen. TEMP has a low detection limit and a relatively long adduct lifetime when compared with other spin traps. This makes it an ideal trap for suspensions containing low concentrations of singlet oxygen that must be irradiated for prolonged periods of time (*40*) for this reason it is widely utilized to detect singlet oxygen (*41, 42*). A mixture of the fullerene colloidal suspension and 80 mM TEMP was shaken in a 5 mL volumetric flask. This was poured into a sample tray for UV irradiation. Upon removal, the sample was taken up in a capillary tube, capped with clay, placed in quartz EPR tube, and positioned in the EPR sample holder. In each case the EPR parameters were held constant as was the TEMP concentration. Separate samples were irradiated under UV for up to 3 h. Signals were compared with the standard product of TEMP and singlet oxygen (TEMPO) in order to determine singlet oxygen generation rate.

2.6. Superoxide Concentration Analysis by XTT. XTT reduction was employed to measure the production of superoxide. The reduction of XTT results in an increase in optical density at 470 nm that can be used to quantify the relative amount of superoxide present (*43, 44*). The concentration of superoxide was determined by comparing XTT reduction with and without a quencher for superoxide, superoxide dismutase (SOD), which allowed nonsuperoxide related XTT reactions to be accounted for. Samples were prepared by mixing 10 mL flasks with the appropriate suspension and 100 μM XTT. One set of experiments was done without SOD while in others, 10 U/mL SOD was added to the samples to quench any superoxide generated. In experiments irradiated by the MP UV lamp, flasks were poured into a Petri dish with surface area approximately 40 cm^2 and depth approximately 1 cm. SOD-containing samples served to eliminate the influence of background absorbance of suspensions at 470 nm. While the physical chemical properties of XTT and TEMP do not favor adsorption to fullerene surfaces, possible interference arising from XTT or TEMP adsorption to aqu/nC_{60} or fullerol aggregates was addressed by adding the compounds in excess as calculated from available fullerene surface area and K_{OW} relationships (see Supporting Information).

2.7. Suspension Preparation. Aqu/nC_{60} was prepared from a supersaturated suspension of C_{60} in water (DDW). Here approximately 0.4 mg/mL of powdered C_{60} was added to DDW. The solution was then stirred and sonicated for approximately 6 h with a Branson sonifier ultrasonic cell disruptor (model S-250A). The final solution had a gold color, characteristic of nC_{60} suspensions, and was filtered through a 0.45 μm methyl cellulose ester (MCE) filter (to remove unsuspended C_{60}) and stored in the dark. The aqu/nC_{60} was also prepared by the same method in D_2O. The final

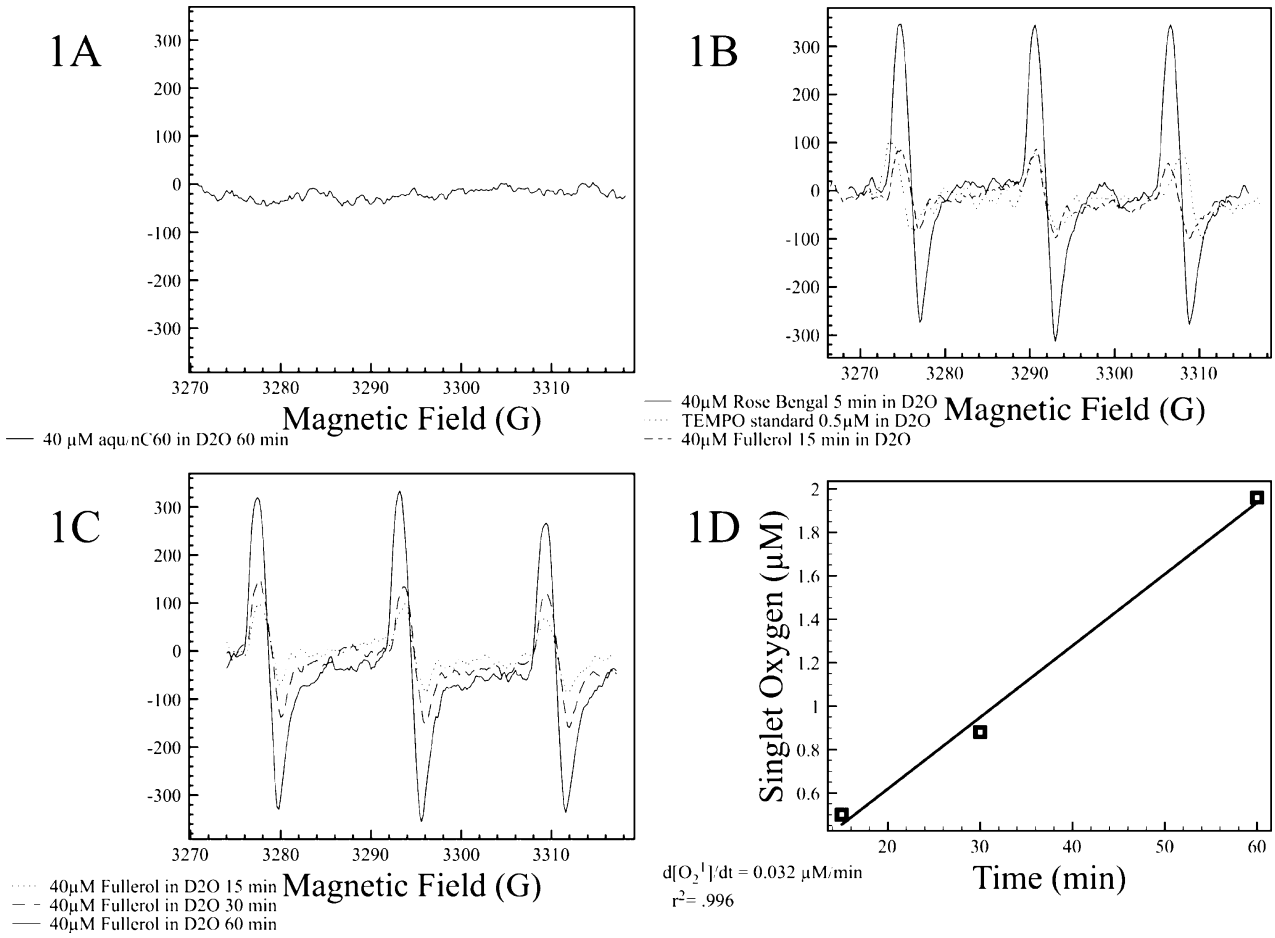

FIGURE 1. A: Electron Paramagnetic Resonance signal between 3270 and 3320 G for a 40 μM aqu/nC$_{60}$ suspended in D$_2$O with 80 mM TEMP and irradiated under LP UV for 60 min. The absence of a triplet signal indicates the absence of singlet oxygen generation.

suspension was found to be stable for periods up to at least 3 months as monitored by mean aggregate size using dynamic light scattering (DLS). In both D_2O and H_2O, the mean diameter of the aqu/nC$_{60}$ was approximately 145 nm as determined by DLS number distribution. Fullerol suspensions were made by adding approximately 0.07 mg/mL powdered fullerol to DDW or D_2O. This suspension was made up in a volumetric flask and placed in the sonication bath for 2 h. During this time the suspension became gradually more gold colored as more fullerol was stabilized in the suspension. Once removed from sonication, the suspension was filtered through 0.45 μm MCE filters via vacuum to remove unsuspended particles. The final suspension contained aggregates with a mean diameter of 200 nm as determined by DLS and a total organic carbon concentration of 90 mg/L. The stock solution was was stable with respect to size and concentration over a period of at least three months. UV/vis absorbance spectra for fullerol and aqu/nC$_{60}$ suspensions have been previously reported (*13, 45*).

3. Results and Discussion

3.1. Singlet Oxygen Production by aqu/nC$_{60}$. EPR measurements were undertaken to compare the singlet oxygen generation capacities of the two types of C_{60} suspensions. Appearance of a distinct triplet signal in an induced magnetic field of the EPR indicates the presence of singlet oxygen (*40*). The aqu/nC$_{60}$ did not produce a signal for the TEMP-singlet oxygen adduct after 60 min of LP UV irradiation, even when these suspensions were made in D_2O to increase detection sensitivity (Figure 1A). These results suggest that aqu/nC$_{60}$ does not participate in detectable type II photosensitization reactions.

1B: Electron Paramagnetic Resonance signal for photosensitizers suspended in D_2O with 80 mM TEMP. Rose Bengal 40 μM and fullerol 40 μM were irradiated with LP UV light. 0.5 μM TEMPO was added as a standard. The field is measured between 3270 and 3320 G.

1C: Electron Paramagnetic Resonance signal for 40 μM Fullerol suspended in D_2O with 80 mM TEMP. The suspension was irradiated under LP UV light for 15, 30, and 60 min. The field is measured between 3270 and 3320 G.

1D: Using the amplitudes of TEMP signals from Figure 1C and the standard signal from 0.05μM TEMPO in Figure 1B the rate of singlet oxygen generation under LP UV is calculated to be 0.032μM/min when 40μM Fullerol suspended in D_2O.

3.2. Singlet Oxygen Production by Fullerol. Deuterated water was also used to increase singlet oxygen sensitivity in experiments with the fullerol suspensions. In contrast with the aqu/nC$_{60}$, fullerol was observed to generate singlet oxygen via the type II photosensitization pathway. The response produced by the fullerol suspension was compared with a standard TEMPO adduct solution and a standard Rose Bengal sensitizing molecule (*21*). Figure 1B compares the signal corresponding to singlet oxygen generation produced by a solution of 40 μM Rose Bengal after 5 min LP UV irradiation with that produced by a separate suspension of 40 μM fullerol following 15 min LP UV irradiation. The Rose Bengal generated singlet oxygen at significantly higher rate than did fullerol. The amplitude of the 0.5 μM TEMPO adduct approximately matches the fullerol signal, meaning that 40 μM fullerol produces approximately 0.5 μM singlet oxygen after 15min of LP UV irradiation.

Singlet oxygen generation with increasing UV fluence is illustrated in Figure 1C where a 40 μM suspension of fullerol

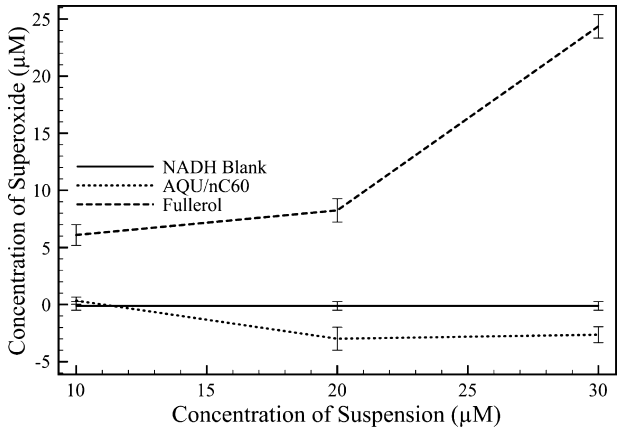

FIGURE 2. Concentration of superoxide radical as a function of XTT (100 μM) absorption at suspension concentrations of 10, 20, and 30 μM. After 5 min of MP UV irradiation fullerol produces more superoxide in the presence of UV light than NADH (500μM) alone. Aqu/nC_{60} produces less superoxide than NADH alone.

was illuminated under UV for 15, 30, and 60 min. From a measurement of signal amplitude and a comparison with the amplitude of the TEMPO standard in Figure 1B an estimate of 0.032 μM/min is obtained for the singlet oxygen generation rate by a 40 μM fullerol suspension under LP UV (Figure 1D).

Singlet oxygen production by fullerol was significant enough to be detected in suspensions of conventional H_2O, but the signal is less distinct and 5 times lower in amplitude for fullerol suspended in water because singlet oxygen has $^1/_{10}$ the lifetime in nondeuterated water. Nonetheless, these measurements confirm significant singlet oxygen production by the fullerol in a water suspension.

3.3. Superoxide Production by Fullerol and aqu/nC_{60} Aggregates. XTT reduction was employed to measure the production of superoxide in the presence of NADH, a common reductant found in cells. As shown in Figure 2 fullerol suspensions generate superoxide in a concentration-dependent manner via type I reaction under medium pressure (MP) UV light. This indicates that the triplet state of fullerol is participating in a type I photosensitization reaction. This is not surprising considering that fullerol participates in type II singlet oxygen production (Figure 1B and C) and with the addition of a donor molecule NADH type I reactions occur by additional reaction steps (Figure 5). On the other hand, it was deduced from the TEMP type II measurements of singlet oxygen (Figure 1A) that aqu/nC_{60} had a short-lived triplet state, possibly due to its aggregation state as we consider subsequently. Therefore, suspensions of aqu/nC_{60} would not be expected to participate in type I photosensitization. This was confirmed by the observation that aqu/nC_{60} experiments produced less superoxide than NADH alone indicating possible antioxidant properties (*9, 46*). It is important to note that since LP and MP UV provided UV fluences that likely differed by 1 order of magnitude, it is impossible to make a direct comparison of type I and type II production rates in this instance.

3.4. TEM and XRD Structural Analysis of Aggregates. Transmission electron microscopy of fullerol aggregates and aqu/nC_{60} show that while both suspensions have a similarly gold-colored appearance, the structure of the aggregates in the suspensions differ greatly (Figure 3). Fullerol suspensions consist of nearly spherical aggregates (n-scale) assembled into larger (m-scale) aggregates of the n-scale spheres. The diameter of a typical n-scale aggregate as observed by TEM (*47*) is slightly smaller than the diameter determined by DLS measurements and may indicate the presence of m-scale aggregates in the suspension. We have previously shown that

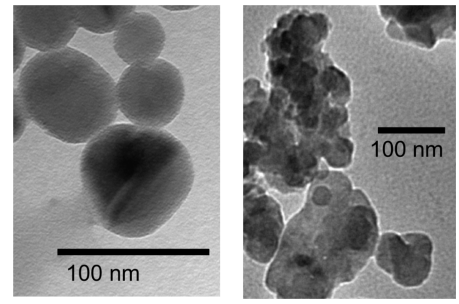

FIGURE 3. TEM images in fullerol aggregates (left) and aqu/nC_{60} (right).

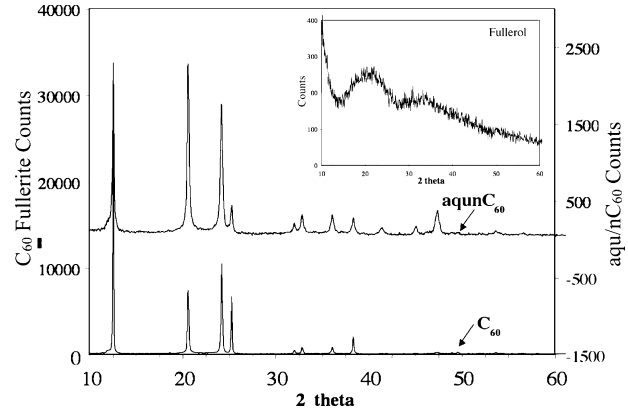

FIGURE 4. XRD diffractogram of C_{60} and aqu/nC_{60} after suspension and drying. Inset: XRD diffractogram of fullerol powder.

the aqu/nC_{60} has a fractal m-scale structure (*45*) reflecting an apparently random assemblage of what appear to be more crystalline n-scale aggregates. However, it is the n-scale structure of the colloidal suspension that will likely determine the proximity of the majority of C_{60}−C_{60} contacts, with implications for the rate of ROS generation due to both the potential for triplet–triplet annihilation, self-quenching, and greater accessibility to the reactive C_{60} surfaces.

Type I and type II photosensitizations by the fullerol and the lack of these reactions with regard to aqu/nC_{60} may indicate a longer lifetime for the triplet state of the hydroxylated C_{60} in the fullerol aggregates compared with that of the aqu/nC_{60} due to differences in structure. XRD was performed on the aggregates in order to obtain an indication of the distance between C_{60} cages, taken to be a qualitative indicator of the rates of triplet–triplet annihilation and self-quenching. In the fullerol diffractogram (Figure 4 inset), the absence of a diffraction peak implies a lack of order within the fullerol aggregate at the n-scale and a greater distance between C_{60} molecules.

In contrast, the aqu/nC_{60} diffractogram (Figure 4) shows a crystalline organization very similar to that of fullerene fine powder (fullerite). C_{60} molecules in aqu/nC_{60} that has been dried into a thin film appear to be assembled in a cubic face centered structure with the same lattice constants as that of C_{60} fullerite ($a = b = c = 14.16$ Å). This organization is apparently retained in spite of the subdivision of particles of the initial C_{60} powder as they form a stable suspension in water. It is reasonable to assume that such a lattice structure is inherited from the original crystal structure of C_{60} fullerite before sonication treatment in water. This tighter n-scale assembly favors triplet–triplet annihilation and reduces the surface of C_{60} effectively available for reaction with approaching oxygen molecules.

3.5. Proposed Framework. We propose a mechanistic framework (Figure 5) derived from literature and experimental evidence to explain the observed trends in ROS production and speciation in large part based on differences

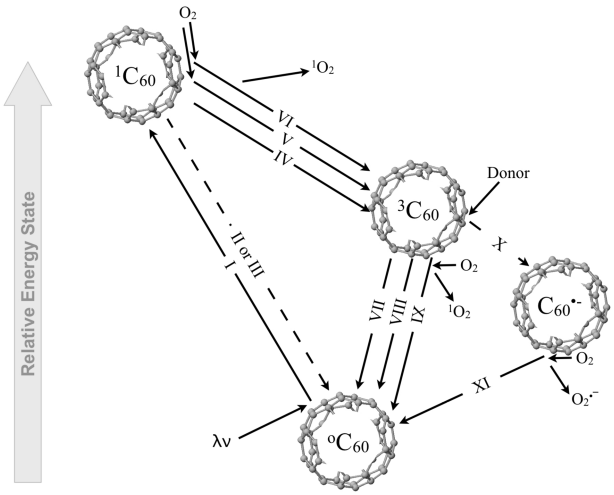

FIGURE 5. Conceptual framework for analysis of fullerene photosensitization and ROS production. Each cage represents the electronic configuration of a generic fullerene molecule (e.g., hydrolylated or underivatized) inside a larger aggregate.

in the structure of aggregates in the aqueous fullerol and nC_{60} suspensions. When fullerenes are illuminated under the appropriate wavelength, the electrons are excited from the ground state ($^oC_{60}$) to the singlet state (I). In the case of aqu/nC_{60} and fullerol, this process likely occurs at a higher rate in aqu/nC_{60} due to a stronger absorbance at UVA wavelengths tested in this study. The singlet state ($^1C_{60}$) can decay in three main manners: fluorescence (II); internal conversion (III); and intersystem crossing (ISC) (IV). The former two pathways return the fullerene to the ground-state while the latter leads to the relaxation of singlet C_{60} to the triplet state ($^3C_{60}$).

Unaltered C_{60} that is found inside aqu/nC_{60} has a high quantum yield for the triplet state (*19*) while altered fullerenes such as fullerol have a lower yield due to cage alteration that promotes fluorescence (II) and internal conversion (III) (*48, 49*). Interaction of the singlet state with oxygen can also result in the triplet state (VI, V). Pathway VI results in the production of singlet oxygen via type II photosensitization while pathway V only results in the formation of the triplet state because energy is released from oxygen in a nonsinglet form. The triplet state, $^3C_{60}$, has a significantly longer lifetime than $^1C_{60}$ in solution allowing it to participate in type II formation of singlet oxygen to a greater extent than does the $^1C_{60}$ (IX). The triplet state is also susceptible to self-quenching (VII) via interaction with the ground state ($^oC_{60}$) and triplet–triplet annihilation (VIII) via interaction with another triplet ($^3C_{60}$). These processes are promoted by close interactions between fullerene cages, and as the XRD data in Figure 4 shows aqu/nC_{60} cages are keeping their tight crystalline form even after suspension, while the fullerol suspensions do not exhibit crystal structure (Figure 4 inset). TEMP measurements of singlet oxygen confirm that the triplet lifetime is significantly different in aqu/nC_{60} which has no trace of type II photosensitization when compared with standards and fullerol suspensions (Figure 1). Along the same lines, type I sensitization (X) occurs when the triplet state comes in contact with a donor molecule (NADH) that has a more negative reduction potential than ($^3C_{60}$). Superoxide measurements in Figure 2 confirm that type I results parallel those found with type II. The resulting radical ($C_{60}^{\bullet-}$) can then pass the electron to ground-state oxygen to form superoxide (XI). Electrons from this radical could also donate to form other types of free radicals such as organic radicals.

The critical agent for producing ROS is the relatively long-lived triplet state (~μs) compared with the short lifetime of the singlet state (~ns) (*19, 50, 51*). Singlet oxygen generation by aqu/nC_{60} measured in Figure 1A validates the proposed mechanism in that aggregates more closely associated with each other (Figure 4) are shown to produce little to no singlet oxygen. Both the hydroxylated (fullerol) and underivatized varieties of C_{60} form stable colloidal suspensions in water. However, aggregation itself does not imply that these fullerenes are not able to produce reactive oxygen. The structure (and likely the size) of the aggregate appear to determine the potential for ROS production. The amorphous structure of the fullerol aggregates favors ROS formation while the tighter and more structured nature of aqu/nC_{60} may prevent ROS production. This occurs despite the higher absorption of UV light at the frequencies exposed and the predicted higher reactivity of the unaltered C_{60} cages (*52*). Accessibility of water to the fullerene surface may also be favored by the fullerol's aggregate structure and hydroxylated functionality compared with the aqu/nC_{60}. These facts, when taken in the context of the proposed mechanism and ROS measurements, indicate that fullerol has a long-lived triplet state in aqueous solution, while aqu/nC_{60} does not. Therefore, the aggregation characteristics affecting triplet lifetime have clear ramifications for the type I and type II photosensitized production of ROS in carbon based nanomaterials and thus should be considered more carefully in future analyses of these materials for toxicity and application in the aqueous environment.

Acknowledgments

EPR assistance was provided by Dr. Marian Fabian at Rice University in Houston, TX. Advice on superoxide detection via XTT was received from Dr. Fridovich at Duke University. Funding support for this work was received from National Science Foundation, US Environmental Protection Agency, and Centre National de la Recherche Scientifique (France).

Supporting Information Available

Calculation and analysis of projected surface area and theoretical K_{OW} values of probes used in this study. This material is available free of charge via the Internet at http://pubs.acs.org.

Literature Cited

(1) Nanotechnology Consumer Products Inventory. http://www.nanotechproject.org/index.php?id=44&action=view&product_id=1132, Accessed August 24, 2007.
(2) Cosmeceuticals, Skin Resuscitating Serum. http://www.sircuitskin.com/inc/pdetail?v=1&pid=2270. Accessed August 24, 2007.
(3) Vitamin C60 Corporation, Antioxidant Face Cream. http://www.vc60.com/english/index.html. Accessed August 24, 2007.
(4) Nakamura, E.; Tokuyama, H.; Yamago, S.; Shiraki, T.; Sugiura, Y. Biological activity of water-soluble fullerenes. Structural dependence of DNA cleavage, cytotoxicity, and enzyme inhibitory activities including HIV-protease inhibition. *Bull. Chem. Soc. Jpn.* **1996**, *69* (8), 2143–2151.
(5) Nakajima, N.; Nishi, C.; Li, F. M.; Ikada, Y. Photo-induced cytotoxicity of water-soluble fullerene. *Fullerene Sci. Technol.* **1996**, *4* (1), 1–19.
(6) Yamago, S.; Tokuyama, H.; Nakamura, E.; Kikuchi, K.; Kananishi, S.; Sueki, K.; Nakahara, H.; Enomoto, S.; Ambe, F. In-Vivo Biological Behavior of a Water-Miscible Fullerene $^-$ C^{14} Labeling, Absorption, Distribution, Excretion and Acute Toxicity. *Chem. Biol.* **1995**, *2* (6), 385–389.
(7) Isobe, H.; Tanaka, T.; Maeda, R.; Noiri, E.; Solin, N.; Yudasaka, M.; Iijima, S.; Nakamura, E. Preparation, purification, characterization, and cytotoxicity assessment of water-soluble, transition-metal-free carbon nanotube aggregates. *Angew. Chem., Int. Ed.* **2006**, *45* (40), 6676–6680.
(8) Xia, T.; Kovochich, M.; Brant, J.; Hotze, M.; Sempf, J.; Oberley, T.; Sioutas, C.; Yeh, J. I.; Wiesner, M. R.; Nel, A. E. Comparison of the abilities of ambient and manufactured nanoparticles to induce cellular toxicity according to an oxidative stress paradigm. *Nano Lett.* **2006**, *6* (8), 1794–1807.

(9) Gharbi, N.; Pressac, M.; Hadchouel, M.; Szwarc, H.; Wilson, S. R.; Moussa, F. [60>]Fullerene is a powerful antioxidant in vivo with no acute or subacute toxicity. *Nano Lett.* **2005**, *5* (12), 2578–2585.
(10) Chiang, L. Y.; Lu, F. J.; Lin, J. T. Free-radical scavenging activity of water-soluble fullerenols. *J. Chem. Soc., Chem. Commun.* **1995**, (12), 1283–1284.
(11) Yu, C.; Bhonsle, J. B.; Wang, L. Y.; Lin, J. G.; Chen, B.-J.; Chiang, L. Y. Synthetic aspects and free-radical scavenging efficiency of polyhydroxylated C_{60}. *Fullerene Sci. Technol.* **1997**, *5* (7), 1407–1421.
(12) Fortner, J. D.; Lyon, D. Y.; Sayes, C. M.; Boyd, A. M.; Falkner, J. C.; Hotze, E. M.; Alemany, L. B.; Tao, Y. J.; Guo, W.; Ausman, K. D.; Colvin, V. L.; Hughes, J. B. C_{60} in water: Nanocrystal formation and microbial response. *Environ. Sci. Technol.* **2005**, *39* (11), 4307–4316.
(13) Brant, J.; Lecoanet, H.; Hotze, M.; Wiesner, M. Comparison of electrokinetic properties of colloidal fullerenes (nC_{60}) formed using two procedures. *Environ. Sci. Technol.* **2005**, *39* (17), 6343–6351.
(14) Vileno, B.; Marcoux, P. R.; Lekka, M.; Sienkiewicz, A.; Feher, I.; Forro, L. Spectroscopic and photophysical properties of a highly derivatized C_{60} fullerol. *Adv. Funct. Mater.* **2006**, *16* (1), 120–128.
(15) Mohan, H.; Palit, D. K.; Mittal, J. P.; Chiang, L. Y.; Asmus, K. D.; Guldi, D. M. Excited states and electron transfer reactions of $C_{60}OH_{18}$ in aqueous solution. *J. Chem. Soc., Faraday Trans.* **1998**, *94* (3), 359–363.
(16) Nagano, T.; Arakane, K.; Ryu, A.; Masunaga, T.; Shinmoto, K.; Mashiko, S.; Hirobe, M. Comparison of singlet oxygen production efficiency of C_{60} with other photosensitizers, based on 1268 nm emission. *Chem. Pharm. Bull. (Tokyo)* **1994**, *42* (11), 2291–2294.
(17) Pickering, K. D.; Wiesner, M. R. Fullerol-sensitized production of reactive oxygen species in aqueous solution. *Environ. Sci. Technol.* **2005**, *39* (5), 1359–1365.
(18) Badireddy, A. R.; Hotze, E. M.; Chellam, S.; Alvarez, P.; Wiesner, M. R. Inactivation of bacteriophages via photosensitization of fullerol nanoparticles. *Environ. Sci. Technol.* **2007**, *41* (18), 6627–6632.
(19) Arbogast, J. W.; Darmanyan, A. P.; Foote, C. S.; Rubin, Y.; Diederich, F. N.; Alvarez, M. M.; Anz, S. J.; Whetten, R. L. Photophysical properties of C_{60}. *J. Phys. Chem.* **1991**, *95* (1), 11–12.
(20) Arbogast, J. W.; Foote, C. S.; Kao, M. Electron-transfer to triplet C_{60}. *J. Am. Chem. Soc.* **1992**, *114* (6), 2277–2279.
(21) Wilkinson, F.; Helman, W. P.; Ross, A. B. Quantum yields for the photosensitized formation of the lowest electronically excited singlet-state of molecular-oxygen in solution. *J. Phys. Chem. Ref. Data* **1993**, *22* (1), 113–262.
(22) Yamakoshi, Y. N.; Yagami, T.; Fukuhara, K.; Sueyoshi, S.; Miyata, N. Solubilization of fullerenes into water with polyvinylpyrrolidone applicable to biological tests. *J. Chem. Soc., Chem. Commun.* **1994**, (4), 517–518.
(23) Hungerbuhler, H.; Guldi, D. M.; Asmus, K. D. Incorporation of C_{60} into artificial lipid-membranes. *J. Am. Chem. Soc.* **1993**, *115* (8), 3386–3387.
(24) Andersson, T.; Nilsson, K.; Sundahl, M.; Westman, G.; Wennerstrom, O. C_{60} Embedded in γ-cyclodextrin—A water-soluble fullerene. *J. Chem. Soc., Chem. Commun.* **1992**, (8), 604–606.
(25) Bensasson, R. V.; Bienvenue, E.; Dellinger, M.; Leach, S.; Seta, P. C_{60} in model biological systems. A visible-UV absorption study of solvent-dependent parameters and solute aggregation. *J. Phys. Chem.* **1994**, *98* (13), 3492–3500.
(26) Chiang, L. Y.; Upasani, R. B.; Swirczewski, J. W. Versatile nitronium chemistry for C_{60} fullerene functionalization. *J. Am. Chem. Soc.* **1992**, *114* (26), 10154–10157.
(27) Nakamura, E.; Isobe, H. Functionalized fullerenes in water. The first 10 years of their chemistry, biology, and nanoscience. *Acc. Chem. Res.* **2003**, *36* (11), 807–815.
(28) Wharton, T.; Kini, V. U.; Mortis, R. A.; Wilson, L. J. New nonionic, highly water-soluble derivatives of C_{60} designed for biological compatibility. *Tetrahedron Lett.* **2001**, *42* (31), 5159–5162.
(29) Deguchi, S.; Alargova, R. G.; Tsujii, K. Stable dispersions of fullerenes, C_{60} and C_{70}, in water. Preparation and characterization. *Langmuir* **2001**, *17* (19), 6013–6017.
(30) Scrivens, W. A.; Tour, J. M.; Creek, K. E.; Pirisi, L. Synthesis of C^{14} Labeled C_{60}, Its Suspension in Water, and Its Uptake by Human Keratinocytes. *J. Am. Chem. Soc.* **1994**, *116* (10), 4517–4518.
(31) Cheng, X. K.; Kan, A. T.; Tomson, M. B. Naphthalene adsorption and desorption from aqueous C_{60} fullerene. *J. Chem. Eng. Data* **2004**, *49* (3), 675–683.
(32) Andrievsky, G. V.; Klochkov, V. K.; Karyakina, E. L.; McHedlov-Petrossyan, N. O. Studies of aqueous colloidal solutions of fullerene C-60 by electron microscopy. *Chem. Phys. Lett.* **1999**, *300* (3–4), 392–396.
(33) Hirsch, A.; Lamparth, I.; Karfunkel, H. R. Fullerene chemistry in 3 dimensions—Isolation of 7 regioisomeric bisadducts and chiral trisadducts of C_{60} and di(ethoxycarbonyl)methylene. *Angew. Chem., Int. Ed.* **1994**, *33* (4), 437–438.
(34) Guldi, D. M.; Asmus, K. D. Activity of water-soluble fullerenes towards •OH-radicals and molecular oxygen. *Radiat. Phys. Chem.* **1999**, *56* (4), 449–456.
(35) Sitharaman, B.; Asokan, S.; Rusakova, I.; Wong, M. S.; Wilson, L. J. Nanoscale aggregation properties of neuroprotective carboxyfullerene (C_3) in aqueous solution. *Nano Lett.* **2004**, *4* (9), 1759–1762.
(36) Brant, J.; Lecoanet, H.; Wiesner, M. R. Aggregation and deposition characteristics of fullerene nanoparticles in aqueous systems. *J. Nanopart. Res.* **2005**, *7* (4–5), 545–553.
(37) Andrievsky, G.; Klochkov, V.; Derevyanchenko, L. Is the C-60 fullerene molecule toxic. *Fullerenes, Nanot., Carbon Nanostruct.* **2005**, *13* (4), 363–376.
(38) Lee, J.; Fortner, J. D.; Hughes, J. B.; Kim, J. H. Photochemical production of reactive oxygen species by C_{60} in the aqueous phase during UV irradiation. *Environ. Sci. Technol.* **2007**, *41* (7), 2529–2535.
(39) Rosenfeldt, E. J.; Linden, K. G. Degradation of endocrine disrupting chemicals bisphenol A, ethinyl estradiol, and estradiol during UV photolysis and advanced oxidation processes. *Environ. Sci. Technol.* **2004**, *38* (20), 5476–5483.
(40) Lion, Y.; Delmelle, M.; Vandevorst, A. New method of detecting singlet oxygen production. *Nature* **1976**, *263* (5576), 442–443.
(41) Martins, J.; Almeida, L.; Laranjinha, J. Simultaneous production of superoxide radical and singlet oxygen by sulphonated chloroaluminum phthalocyanine incorporated in human low-density lipoproteins: Implications for photodynamic therapy. *Photochem. Photobiol.* **2004**, *80* (2), 267–273.
(42) Yamakoshi, Y.; Umezawa, N.; Ryu, A.; Arakane, K.; Miyata, N.; Goda, Y.; Masumizu, T.; Nagano, T. Active oxygen species generated from photoexcited fullerene (C_{60}) as potential medicines: $O_2^{-\bullet}$ versus O_2^1. *J. Am. Chem. Soc.* **2003**, *125* (42), 12803–12809.
(43) Ukeda, H. H.; Maeda, S. S.; Ishii, T. T.; Sawamura, M. M. Spectrophotometric assay for superoxide dismutase based on tetrazolium salt 3′−1−(phenylamino)-carbonyl−3, 4-tetrazolium]-bis(4-methoxy-6-nitro)benzenesulfonic acid hydrate reduction by xanthine-xanthine oxidase. *Anal. Biochem.* **1997**, *251* (2), 206–209.
(44) Bartosz, G. Use of spectroscopic probes for detection of reactive oxygen species. *Clin. Chim. Acta* **2006**, *368* (1–2), 53–76.
(45) Brant, J. A.; Labille, J.; Bottero, J. Y.; Wiesner, M. R. Characterizing the impact of preparation method on fullerene cluster structure and chemistry. *Langmuir* **2006**, *22* (8), 3878–3885.
(46) Wang, I. C.; Tai, L. A.; Lee, D. D.; Kanakamma, P. P.; Shen, C. K. F.; Luh, T. Y.; Cheng, C. H.; Hwang, K. C. C_{60} and water-soluble fullerene derivatives as antioxidants against radical-initiated lipid peroxidation. *J. Med. Chem.* **1999**, *42* (22), 4614–4620.
(47) Brant, J. A.; Labille, J.; Robichaud, C. O.; Wiesner, M. Fullerol cluster formation in aqueous solutions: Implications for environmental release. *J. Colloid Interface Sci.* **2007**, *314* (1), 281–288.
(48) Bensasson, R. V.; Bienvenue, E.; Janot, J. M.; Leach, S.; Seta, P.; Schuster, D. I.; Wilson, S. R.; Zhao, H. Photophysical properties of 3 hydrofullerenes. *Chem. Phys. Lett.* **1995**, *245* (6), 566–570.
(49) Anderson, J. L.; An, Y. Z.; Rubin, Y.; Foote, C. S. Photophysical characterization and singlet oxygen yield of a dihydrofullerene. *J. Am. Chem. Soc.* **1994**, *116* (21), 9763–9764.
(50) Wasielewski, M. R.; Oneil, M. P.; Lykke, K. R.; Pellin, M. J.; Gruen, D. M. Triplet-states of fullerenes C_{60} and C_{70}—Electron-paramagnetic resonance-spectra, photophysics, and electronic-structures. *J. Am. Chem. Soc.* **1991**, *113* (7), 2774–2776.
(51) Haufler, R. E.; Wang, L. S.; Chibante, L. P. F.; Jin, C. M.; Conceicao, J.; Chai, Y.; Smalley, R. E. Fullerene triplet-state production and decay—R2pi Probes of C_{60} and C_{70} in a supersonic beam. *Chem. Phys. Lett.* **1991**, *179* (5–6), 449–454.
(52) Hamano, T.; Okuda, K.; Mashino, T.; Hirobe, M.; Arakane, K.; Ryu, A.; Mashiko, S.; Nagano, T. Singlet oxygen production from fullerene derivatives: Effect of sequential functionalization of the fullerene core. *Chem. Commun.* **1997**, (1), 21–22.

ES702172W